# Role of oxygen concentrations on structural and optical properties of RF magnetron sputtered ZnO thin films

**7 authors**, including:

Francis Otieno
University of the Witwatersrand
**20** PUBLICATIONS **93** CITATIONS

SEE PROFILE

Mildred Awuor Airo
University of the Witwatersrand
**27** PUBLICATIONS **209** CITATIONS

SEE PROFILE

Theodore Ganetsos
University of West Attica
**77** PUBLICATIONS **453** CITATIONS

SEE PROFILE

Rudolph Marthinus Erasmus
University of the Witwatersrand
**125** PUBLICATIONS **1,837** CITATIONS

SEE PROFILE

Some of the authors of this publication are also working on these related projects:

Hybrid Perovskites View project

Chemical Crystallography View project

# Role of oxygen concentrations on structural and optical properties of RF magnetron sputtered ZnO thin films

Francis Otieno[1,2,5] · Mildred Airo[3] · Theodore Ganetsos[4] · Rudolph M. Erasmus[1,2] · David G. Billing[1,3] · Alexander Quandt[1,2,5] · Daniel Wamwangi[1,2,5]

## Abstract

We report an investigation on the effect of oxygen flow rate on the structural and optical properties of zinc oxide thin films prepared by RF magnetron sputtering. The structural measurements were carried using grazing incidence X-ray diffraction, atomic force microscopy and Raman spectroscopy. The role of oxygen partial pressure on the crystallinity, the surface morphology and vibrational modes has been established. The optical properties of the films were investigated using FR-Basic-VIS/NIR fitted with FR-Monitor software for film thickness, refractive index and color determination. The film thickness is observed to increase when oxygen is introduced at 4 sccm but eventual decrease with increase in the flow rate an indication of initial increase in rate of deposition followed by reduction. Elaborate explanations of these trends are provided.

**Keywords** Zinc oxide · Photo-luminescence · Thin films · Raman

## 1 Introduction

Zinc oxide (ZnO) is a semiconductor in the II–VI group with ionicity at the borderline between covalent and ionic semiconductors. The crystal structures shared by ZnO are wurtzite B4, zinc blende B3, and rocksalt B1 (Özgür et al. 2005). It is believed to have a lot of promising device applications due to its multiple excellent properties. Initially ZnO was considered as a substrate for GaN and other related alloys (Janotti et al. 2009; Lupan et al. 2010). At ambient

✉ Daniel Wamwangi
daniel.wamwangi@wits.ac.za

1 Materials for Energy Research Group, University of the Witwatersrand (Wits), Private Bag 3, Johannesburg 2050, South Africa

2 Material Physics Research Institute, School of Physics, University of the Witwatersrand (Wits), Private Bag 3, Johannesburg 2050, South Africa

3 School of Chemistry, University of the Witwatersrand (Wits), Private Bag 3, Johannesburg 2050, South Africa

4 University of West Attica, Perou Ralli & Thevon 250, Egaleo, Greece

5 Historical Museum of Physics and Study and Research Centre "Enrico Fermi", 00184 Rome, Italy

conditions, ZnO possesses thermodynamically stable phase of a Wurtzite structure similar to GaN (Özgür et al. 2005; Karpina et al. 2004), a factor that makes it widely applicable in high-performance optoelectronic devices. The increased research on zinc oxide as a semiconductor material is majorly driven by its prospective use as a wide band gap semiconductor for light emitting devices and for transparent or high temperature electronics (Nomura et al. 2003). It has a direct and wide band gap of 3.37 eV (at 300 K) in the near-UV spectral region, a large free-exciton binding energy (60 meV) such that excitonic emission processes can persist at or even above room temperature (Thomas 1960; Chen et al. 1998; Reynolds et al. 1999), a strong cohesive energy of 1.89 eV (Chuang et al. 2007), with a high optical gain (300 cm$^{-1}$) (Chen et al. 1998). In addition it exhibits high mechanical strength, thermal stability, chemical stability, ambient insensibility, and negative electron affinity (Wang et al. 2005) as well as high radiation hardness (Look et al. 1999). These characteristics of ZnO as well as unique combination of its physical properties—optical, electrical, magnetic, piezoelectric, and ferroelectric properties make it a promising candidate material for advanced devices applications. Different commercial applications have also been reported such as integrated optics, antireflection coatings, liquid crystal displays (Özgür et al. 2005), light emitting, laser diodes (Willander et al. 2009; Pauporté et al. 2006), *U-V* range detecting devices (Lupan et al. 2008a, b, 2009a, b), chemical sensors, solar cells (Lupan et al. 2008a, b, 2009a, b; Yoshida et al. 2009), photodegradation and photocatalysis (Pauporte and Rathouský 2007), superhydrophobic and self-cleaning surfaces. According to (Badre et al. 2007), ZnO films possess superhydrophobic properties over a wide pH range with excellent stability under high temperature and ambient long-term storage conditions making it a strong candidate for high temperature electronic devices that can reliably be operated in space and other harsh environments. There are several techniques of attaining ZnO thin films such as Pulse Laser Deposition, chemical vapour deposition (CVD), spray pyrolysis and magnetron sputtering. The latter is usually preferred due to various advantages including: low substrate temperatures (down to room temperature), good adhesion of films on substrates, high deposition rates (up to 12 μm min$^{-1}$) (Kukla et al. 1990), very good thickness uniformity and high density of the films, Good controllability and long-term stability of the process, relatively cheap deposition method as well as ability to scale to large areas (up to 3×6 m$^2$) (Szczyrbowski et al. 1989). Generally, the structure and optical properties of sputtered films are strongly influenced by gas composition (Hong et al. 2005).

In order to obtain stoichiometric ZnO film, it is necessary to optimize sufficient amount of oxygen with argon in the sputtering system. The ZnO thin films reported here were first deposited with Ar flow rate of 13 sccm without oxygen then later introduced oxygen ambient at different flow rates to suppress the oxygen vacancies that act as annihilators of holes during film deposition. Oxygen partial pressure or flow rate showed great influence on the deposition rate of ZnO. It has been reported that addition of Oxygen during RF sputtering process is important for obtaining a semiconducting ZnO film and that no oxygen or too much oxygen can make the ZnO film either metallic or insulating (Chiu et al. 2011). An increase of the oxygen flow rate in the working gas reduces the number of incident Ar atoms which can transfer their high energy to the target. Therefore, the growth rate for ZnO films decreases with increasing oxygen concentration.

## 2 Experimental procedure

### 2.1 Thin films growth conditions

ZnO films were deposited by R.F. magnetron sputtering system using a cylindrical metallic ZnO disc 76 mm diameter and 3–6 mm thick as the cathode (99.95% purity, from Semiconductor Wafer Inc.). Substrate used was a p-type silicon with (100) orientation. The substrates were thoroughly cleaned with organic solvents and dried before loading in the sputtering system. The vacuum chamber was evacuated to a roughing pressure of $2 \times 10^{-2}$ mbar before a further pump down to a base pressure of $1.8 \times 10^{-5}$ mbar. Magnetron sputtering was carried out in an argon and oxygen gas atmosphere supplied into the chamber through a constant precision leak valve at a flow rate of 13.0 sccm and a variable 0–15 sccm, respectively.

### 2.2 Characterization techniques

The surface morphology and the root-mean-square (rms) surface roughness of the films were characterized using a Di100 model atomic force microscope (AFM) in tapping mode. The crystallographic properties of the ZnO films was carried out using GXRD Bruker D8 Discover, 40 kV, 40 mA using a 8.0 keV Cu-Kα radiation. The scanning range of 2θ was varied from 10° to 80° at a low scanning rate of 1.2°/min. The Raman bands and the structural order of all the films were examined using a Horiba LabRAM HR Raman spectrometer equipped with an Ar ion laser (514.5 nm) and a laser power of < 1 mW at the sample. Optical reflectance to attain thickness, refractive index, colour were analyzed using FR-Basic-VIS/NIR fitted with FR-Monitor software for fittings. The calculation to obtain thickness, refractive index and colour was performed through fitting of the experimental reflectance spectrum by applying the ThetaMetrisis's proprietary physical models that are implemented through appropriate algorithms which in our case the Levenberg–Marquardt was used.

## 3 Results and discussions

### 3.1 Surface topography of ZnO films by atomic force microscopy

Figure 1 shows the morphologies of the obtained ZnO thin films deposited with different oxygen flow rates. It was clearly observed that all of the films exhibited a flat and uniform surface topography. The grain size and roughness were also obtained from the AFM as tabulated in Table 1. The film deposited without Oxygen in the chamber showed a roughness of 17.8 nm and a grain size of 46.7 nm. These values slightly increased to 19.9 nm and 47.8 nm respectively at 4 sccm Oxygen flow rate. This is in agreement with the increase in the deposition rate witnessed from the thickness measurements. At 8 sccm oxygen flow rate and beyond, the grain size and roughness decreased giving variation in film colour as shown in the top right corner of each AFM image and summarized in CIE colour diagram of Fig. 1.

The introduction of the high-energy negative oxygen ions bombardments may be responsible for the increase of the roughness since it degrades the surface quality of the film (Table 1).
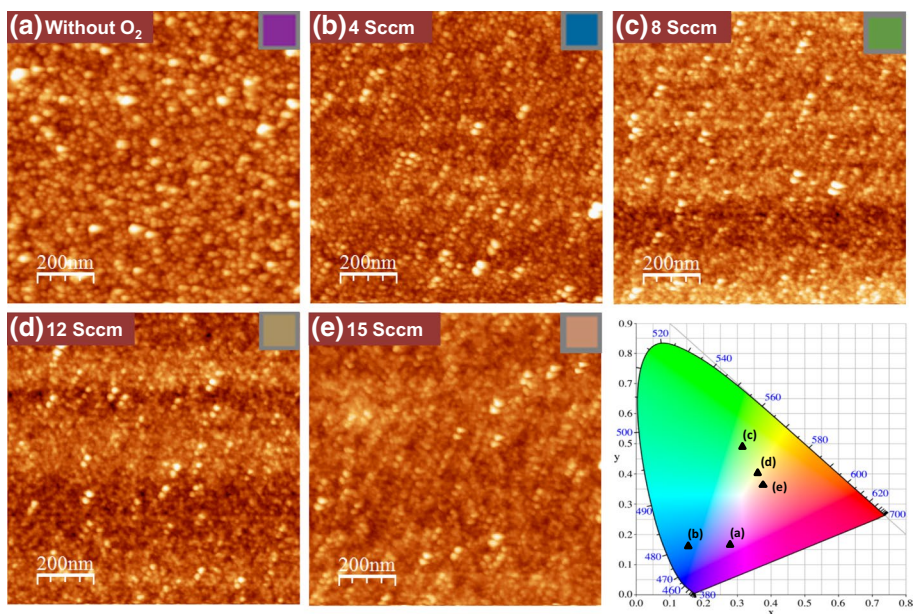
**Fig. 1** AFM (tapping mode) image of films grown at different oxygen flow rate and CIE diagram

**Table 1** Summary of tapping mode AFM analysis for films deposited at different oxygen flow rate with constant Ar flow rate of 13 sccm

| $O_2$ flow rate (sccm) | $R_{rms}$ (nm) | Skewness ($R_{sk}$) | Grain height (nm) |
|---|---|---|---|
| 0 | 17.8 | 0.605 | 46.7 |
| 4 | 19.9 | 0.470 | 47.9 |
| 8 | 18.3 | 0.558 | 46.4 |
| 12 | 15.1 | 0.512 | 42.2 |
| 15 | 16.2 | 0.724 | 40.1 |

Figure 1 also shows the Commission Internationale de l'Eclairage (CIE) (Kumar et al. 2014) parameters, colour coordinate (x–y) calculated in an attempt to establish the change in the photometric characteristics of the ZnO thin films deposited at the different oxygen flow rates. The CIE chromaticity diagram was calculated using the FR-Basic-Vis/NIR fitted with FR fitting tool with colour calculator software. It can be seen from the figure that the CIE coordinates (x, y) of (0.292, 0.161) for thin film without Oxygen in the chamber. All films had colour coordinates in close proximity to the locus of points following the line of a black-body-radiator.

The elemental composition of the films shows that there was no external impurity during the growth as well as at characterization stage as observed in the EDS in Fig. 2. This lack of impurity phases was also confirmed by GIXRD peaks shown in Fig. 3.
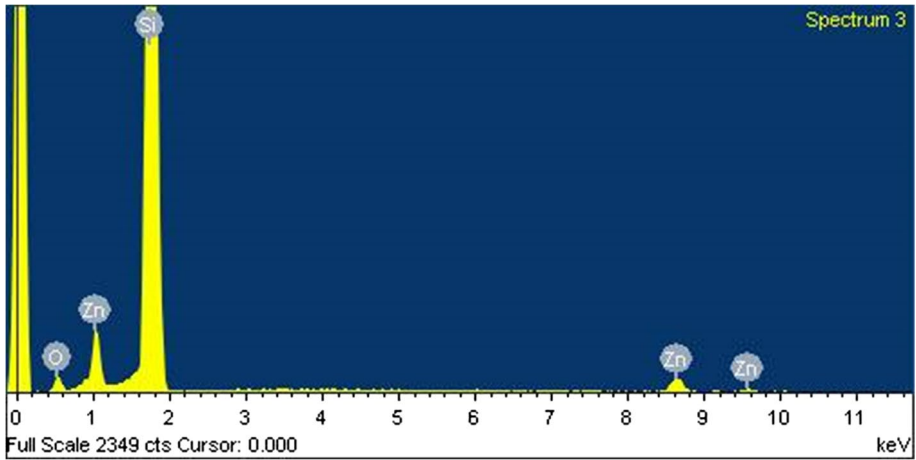
**Fig. 2** EDS analysis of the ZnO thin film grown using RF sputtering on Si wafer substrate

**Fig. 3** GIXRD pattern of ZnO thin films grown using different oxygen flow rate. Inset is a zoom of the (002) peak
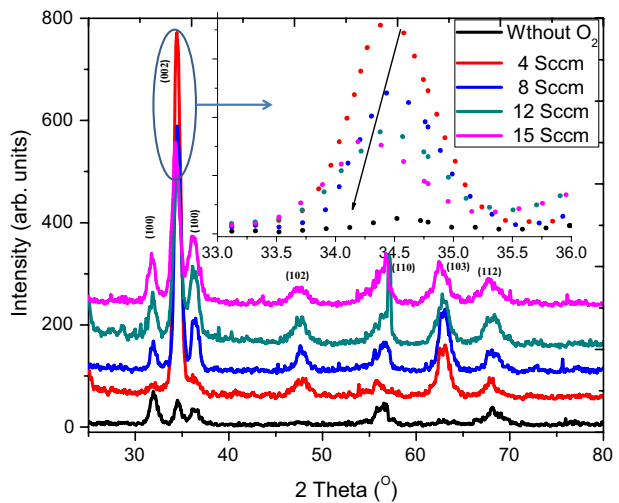


## 3.2 XRD analysis

The GIXRD patterns of the ZnO thin films deposited at different oxygen flow rate appear in Fig. 3. All the peaks are indexed to the JCP2 card number 003–0888 with a hexagonal wurtzite structure of the space group of P63mc and lattice constants, $a = 3.2489$ Å and $c = 5.2062$ Å.

The peak intensity and full width at half maximum were also calculated from the (002) peak and the results reported in Fig. 4. From analysis, the peak intensity is seen to increase when oxygen is introduced at 4 sccm then assumes a reducing trend as the flow rate increases. The FWHM on the other hand reduces when a flow rate of 4 sccm is used before increasing with oxygen flow rate. Generally, the (002) diffraction peak shifted to lower angle and broadened as oxygen flow rate increased suggesting that the film crystallization
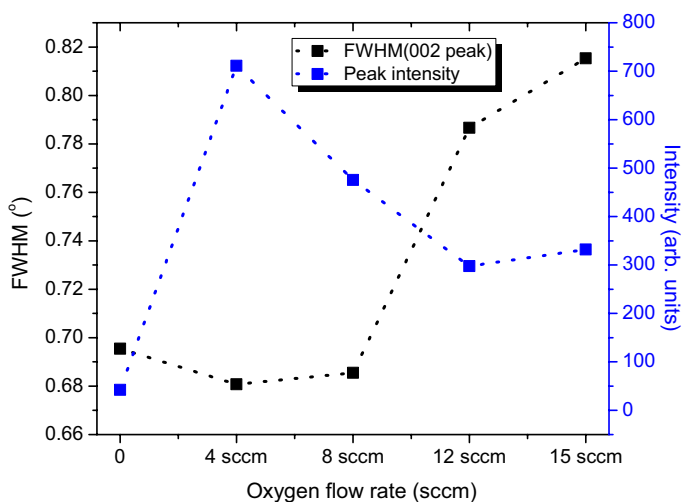
**Fig. 4** Variation of the (002) FWHM and peak intensity with oxygen flow rate

deteriorated with impinging higher energy species as magnetron sputtering plasma suppressed the sputtering efficiency.

We further carried out multi-peak fitting using Origin8 software (originLab corporation) such that the peak center positions could be calculated and used to derive the lattice spacing using Bragg's relation:

$$\lambda = 2d_{hkl}\text{Sin}\theta_{hkl} \tag{1}$$

where $\theta$ is the Bragg's angle (angle between normal to the diffracting plane and incident X-ray), $\lambda$ is the X-ray wavelength which in our case was CuK$\alpha$ radiation with a wavelength of 1.541 Å (Table 2). The lattice parameters a and c were obtained for the (002) peaks using the expression for a hexagonal system (Iqbal et al. 2015).

$$\frac{1}{d^2} = \frac{4}{3}\left(\frac{h^2 + hk + l^2}{a^2}\right) + \frac{l^2}{c^2} \tag{2}$$

The dislocation density δ, defined as the length of dislocation lines per unit volume of the crystal (Williamson and Smallman) and the strain present in thin film were investigated using Eqs. 3 and 4 respectively (Otieno et al. 2017).

**Table 2** Estimated peak center position, lattice parameters, dislocation density and strain from XRD data

| Oxygen flow rate (sccm) | (002) Position | FWHM (nm) | a/(Å) | C/(Å) | δ (10^15) | ε (10^−3) |
|---|---|---|---|---|---|---|
| 0 | 34.56 | 0.696 | 2.99 | 5.19 | 6.99 | 2.90 |
| 4 | 34.47 | 0.681 | 3.00 | 5.20 | 6.69 | 2.83 |
| 8 | 34.43 | 0.686 | 3.01 | 5.21 | 6.79 | 2.85 |
| 12 | 34.31 | 0.787 | 3.02 | 5.22 | 8.95 | 3.28 |
| 15 | 34.27 | 0.815 | 3.02 | 5.23 | 9.62 | 3.40 |

$$\delta = \frac{1}{D_{sh}^2} \tag{3}$$

$$\varepsilon = \frac{\beta \cos\theta}{4} \tag{4}$$

The strain in the films initially relaxes at 4 sccm probably an indication of less defects in the lattice or reduction of grain boundary energy at the grain boundary. As the oxygen concentration increases the strain increases such that there is an increase in the interplanar spacing d variation leading to the increase in dislocation density. The increasing strain and dislocation density together reduces the stoichiometry of the films, which in turn causes the volumetric contraction of the thin films leading to a deterioration of films crystallinity as also ascertained by the FWHM results (Thanikaikarasan et al. 2009).

### 3.3 Raman studies on oxygen variation

Figure 5 shows Raman measurements in the backscattering geometry used to identify Raman active modes with variation in oxygen concentration at a constant Ar flow rate of 13 sccm. ZnO thin films grown by RF sputtering exhibit a wurtzite structure with four atoms per unit cell giving rise to 12 phonons, 9 optical and 3 acoustic branches/modes namely: longitudinal acoustic (LA), transverse-acoustic (TA), longitudinal-optical (LO), and transverse-optical (LO) branch. Group theory predicts that near the center of the Brillouin zone there is an optical phonon, $\Gamma = A_1 + 2B_1 + E_1 + 2E_2$. The A1 and a doubly degenerate E1 branches are Raman and infrared active, while the two double degenerate $E_2$ branches (nonpolar) are Raman active only (Du et al. 2008). The $E_2$ low mode is associated with the vibrations of the Zn sub-lattice, while the $E_2$ high mode is associated with the oxygen atoms only (Youssef et al. 2008). The B branches are always inactive.



**Fig. 5** Raman spectroscopy of ZnO thin films grown at different $O_2$ concentrations
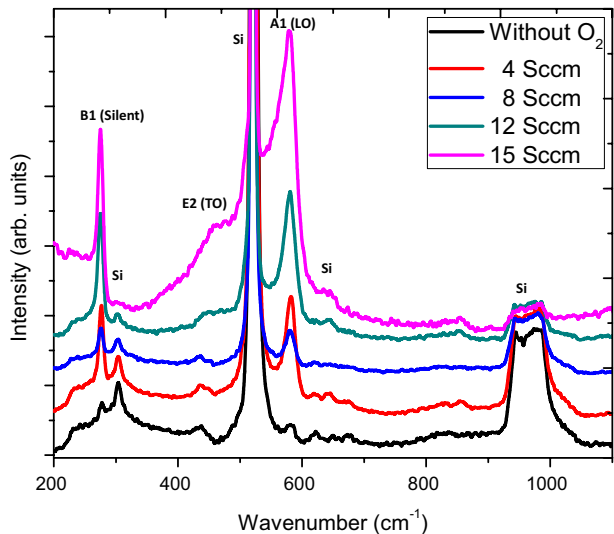
The Ar flow was kept constant at 13 sccm while the $O_2$ flow was varied from 0 to 15 sccm. At 0 sccm $O_2$ flow, Raman shift peaks were observed at 272 cm$^{-1}$, 303 cm$^{-1}$, 435 cm$^{-1}$, 522 cm$^{-1}$, 581 cm$^{-1}$, and a broad peak stretching from 941 to 992 cm$^{-1}$.

Appearance of the peak near 272 cm$^{-1}$ could be attributed to the B1 silent inactive mode while the peak near to 435 cm$^{-1}$ could be attributed to Raman active phonon mode E2 (TO). Another mode observed around 581 cm$^{-1}$ could be attributed to E1 (LO) branch (Saravanakumar et al. 2011). These optical phonon modes confirm that the RF magnetron sputtered polycrystalline thin films have the wurtzite hexagonal phase. According to Tzolov et al. (2001), the observation of bands near 272 and 581 cm$^{-1}$ are common in ZnO thin films and not seen in the Raman spectra of ZnO single crystal and of ZnO polycrystalline material could be attributed to the presence of a depletion region within the crystallites in the ZnO thin films. Such depletion region has an electric field usually formed by charge trapping of free carriers either on defect interface states or on ionized adsorbates at the grain boundaries creating an enhanced LO band and the silent mode. Increasing the Oxygen flow leads to enhancement of these peak intensity. According to Levinson's model (Levinson et al.1982), charge mobility decreases with increasing oxygen flow rate. The mobility of charge carriers is given by Eq. (5):

$$\mu^{-1} = \mu_o^{-1} + [\mu_{gb} \exp(-E_b/KT)]^{-1} \tag{5}$$

where $\mu_o$ is the mobility of a crystalline ZnO grain and $\mu_{gb} \exp(-E_b/KT)$ is the contribution giving grain-boundary scattering. $E_b$ is the barrier height and is proportional to $N_t^2/\varepsilon n$, $N_t$ being the density of traps in the grain boundary, $\varepsilon$ is the ZnO the dielectric constant while n is the density of mobile carriers in a grain.

When the oxygen flow rate increases, more oxygen is absorbed in the grain boundaries, acting as deep trap states for free electrons. The relative grain boundary trap density can be estimated using equation (ii):

$$N_t^2(x) = \ln \left[ \frac{\mu_o}{\mu_{(x)}} - 1 \right] \tag{6}$$

where $N_t$ is the density of traps in the grain boundary, x refers to oxygen flow rate, $\mu_o$ is the mobility in a crystalline ZnO grain approximately 200 cm$^2$/Vs while $\mu$ is the mobility in a polycrystalline ZnO grain (Huang et al. 2014).

The Raman peaks at about 435 cm$^{-1}$ is assigned to the non-polar optical phonons $E_2$ (high) modes of the ZnO thin films. This peak intensity reduces as Oxygen concentration increases and is red shifted. The vanishing is an indication that the oxygen-rich environment playing a great role in reducing the defect states. On the other hand the red shifting indicates a change in stress within the films.

The peaks at about 303, 522 and 960 cm$^{-1}$ are attributed to the optical phonon modes of the silicon substrate. Silicon possesses the diamond structure $O_h^7$ (Fd3m) and therefore has only one first-order Raman-active phonon of symmetry $\Gamma_{25}$ which is located at the Brillouin-zone center. The first order Raman (stokes) spectrum consists of one strong peak at 522 cm$^{-1}$ arising from the creation of the triply degenerate, long wavelength transverse optical phonon (TO) (Spizzirri et al. 2010). The second order Raman (2TO mode) is observed around 941–992 cm$^{-1}$ and is attributed to the convolution of the second order Raman bands of the ZnO thin films with the silicon substrate.

## 3.4 VIS/NIR analysis

Figure 6 shows reflectance measurements obtained from FR-Basic-Vis/NIR spectroscopy over a wavelength range of 450–900 nm. Whenever electromagnetic wave such as light crosses the interface between two different materials, the fraction of light is reflected by the inner surface while some amount of electromagnetic wave is refracted through the inner surface and finally transmitted (Sultan and Sultana 2015).

Figure 6 shows the optical reflectance spectra of ZnO films grown with different oxygen flow rate into the RF chamber over spectral range 450–900 nm. The well-developed interference patterns are an indication that the films are specular to a great extent. Interference fringes with minima and maxima as a result of interference fringes brought about by multiple reflections of light occurring between the lower surface in contact with the substrate and the free surface of the layer are reported. The shifting of these minima and maxima is indication of varying film thickness as reported by the peak fitting shown in Fig. 6. The fitting was carried out using FR tool software with high accuracy (<0.2% error).

From the spectrum fitting shown in Fig. 7, the film thickness variation, an indication of varying deposition rate at different Oxygen flow rate into the chamber was calculated and results summarized in Fig. 8. It is further seen that the introduction of Oxygen changes the refractive index within the visible region.

Thickness of the films deposited without Oxygen into the chamber was 193.8 nm. Upon introduction of oxygen at a rate of 4 sccm, the thickness first increased to 223.5 nm based on the simulation of the reflectance spectra. The optical density in the modelled optical constants has decoupled from the film thickness using independent FESEM measurements. The FESEM image of Fig. 9 has yielded an average film thickness of $230 \pm 10$ nm. This indication of increased deposition rate could be as a result of rapid oxidation of the target and since the oxides targets have a higher secondary electron yield compared to the metal targets, this could have resulted into more ionization of the sputtering gas hence an increase in the deposition rate (Valliyil Sasi et al. 2017). The oxidation reaction likely to
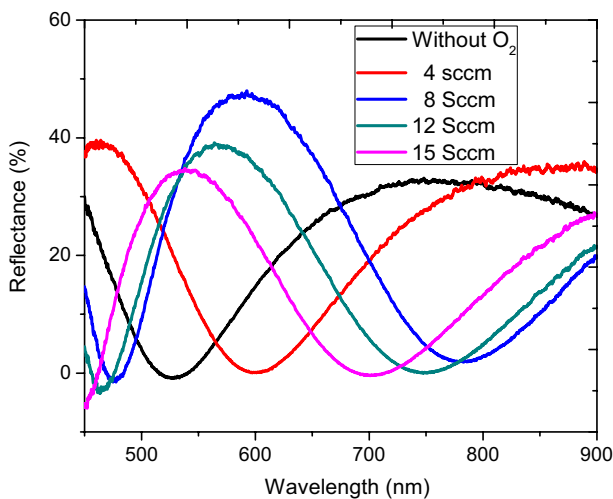


**Fig. 6** Optical reflectance spectrum of ZnO thin film deposited using different oxygen flow rates into the RF chamber
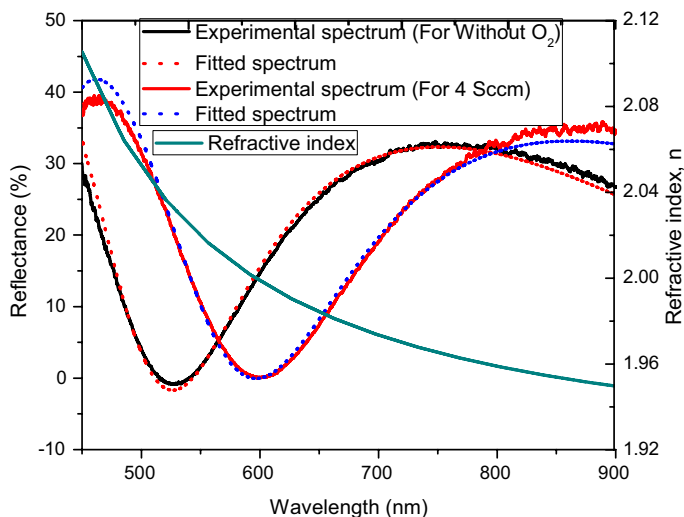
**Fig. 7** Spectrum fitting to derive thickness of the film and refractive index
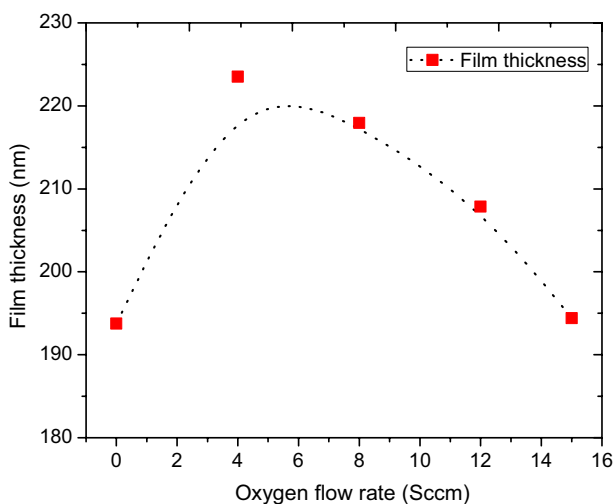


**Fig. 8** Film thickness variation with oxygen flow rate

take place at the substrate surface as described by equation: $2Zn + O_2 = 2ZnO$ (Zhang et al. 2007). At this oxygen flow rate we observe highest peak intensity and minimum FWHM implying highest film crystallinity, this is because at this point the species deposited on the substrate are fully oxidized hence Zn:O ratio may be stoichiometric. At 8, 12 and 15 sccm there was a general decrease in film thickness to 217.9 nm, 207.8, and 194.4 nm respectively, an indication of declining rate of deposition. This reduction in the deposition rate can be explained in two aspects. The first scenario is that the further increase in the oxygen concentration forms a surface layer of adsorbed oxygen, which prevents the sputtering of
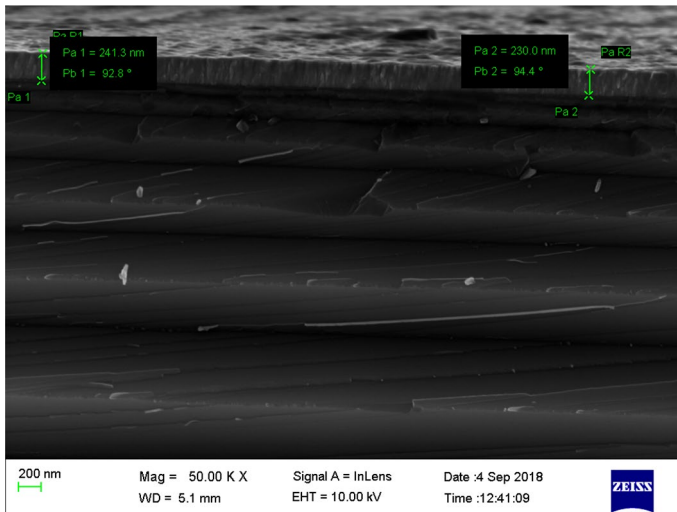
**Fig. 9** Field emission scanning electron microscope image of ZnO thin film grown at oxygen flow rate of 4 sccm

the atoms and thus reduces the deposition rate. The second as reported by Li et al. (2013), as the oxygen concentration increases in the chamber, the concentration of the heavier Ar atoms decreases which could negatively affect the deposition rate. According to Tominaga et al. (1982) oxygen in the RF plasma exist as negative ion, which contributes to neutralization in plasma on the way to the anode (Nagata et al. 2004). This electron-negative species nature of Oxygen may also lead to higher electron-temperature plasma (Jie et al. 2010). The increase in the plasma neutralization with oxygen concentration results in decrease in the amount of Ar ions hence decrease in the deposition rate.

## 4 Conclusion

ZnO thin films have been grown on Si (100) substrates using radio-frequency magnetron from ZnO target. The effect of varied oxygen flow rate into RF sputtering chamber with constant Ar flow of 13 sccm on the structural and optical properties has been investigated. From the GIXRD analysis, the C-axis preferential orientation is sensitive to the oxygen flow rate. From optical analysis, the film thickness first increased as a result of the ZnO oxidization then assumes a decreasing trend. We have also shown that the growth ambient has a strongly influence on the emission characteristics of ZnO films.

# References

Badre, C., Pauporté, T., Turmine, M., Lincot, D.: A ZnO nanowire array film with stable highly water-repellent properties. Nanotechnology **18**, 365705 (2007)

Chen, Y., Bagnall, D., Koh, H.-J., Park, K.-T., Hiraga, K., Zhu, Z., Yao, T.: Plasma assisted molecular beam epitaxy of ZnO on c-plane sapphire: growth and characterization. J. Appl. Phys. **84**, 3912–3918 (1998)

Chiu, C., Pei, Z., Chang, S., Chang, S., Chang, S.: Effect of oxygen partial pressure on electrical characteristics of amorphous indium gallium zinc oxide thin-film transistors fabricated by thermal annealing. Vacuum **86**, 246–249 (2011)

Chuang, R.W., Wu, R.-X., Lai, L.-W., Lee, C.-T.: ZnO-on-GaN heterojunction light-emitting diode grown by vapor cooling condensation technique. Appl. Phys. Lett. **91**, 231113-1–231113-3 (2007)

Du, Y.-P., Zhang, Y.-W., Sun, L.-D., Yan, C.-H.: Efficient energy transfer in monodisperse Eu-doped ZnO nanocrystals synthesized from metal acetylacetonates in high-boiling solvents. J. Phys. Chem. C **112**, 12234–12241 (2008)

Hong, R., Qi, H., Huang, J., He, H., Fan, Z., Shao, J.: Influence of oxygen partial pressure on the structure and photoluminescence of direct current reactive magnetron sputtering ZnO thin films. Thin Solid Films **473**, 58–62 (2005)

Huang, J.: Zinc oxide thin film transistors by radio frequency magnetron sputtering, pp. 7–47 (2014)

Iqbal, A., Zakria, M., Mahmood, A.: Structural and spectroscopic analysis of wurtzite $(ZnO)_{1-x}$ $(Sb_2O_3)_x$ composite semiconductor. Prog. Nat. Sci. Mater. **25**, 131–136 (2015)

Janotti, A., Van de Walle, C.G.: Fundamentals of zinc oxide as a semiconductor. Rep. Prog. Phys. **72**, 126501-1–126501-29 (2009)

Jie, J., Morita, A., Shirai, H.: Role of oxygen atoms in the growth of magnetron sputter-deposited ZnO films. J. Appl. Phys. **108**, 033521-1–033521-8 (2010)

Karpina, V., Lazorenko, V., Lashkarev, C., Dobrowolski, V., Kopylova, L., Baturin, V., Pustovoytov, S., Karpenko, A.J., Eremin, S., Lytvyn, P.: Zinc oxide–analogue of GaN with new perspective possibilities. Cryst. Res. Technol. **39**, 980–992 (2004)

Kukla, R., Krug, T., Ludwig, R., Wilmes, K.: A highest rate self-sputtering magnetron source. Vacuum **41**, 1968–1970 (1990)

Kumar, V., Som, S., Kumar, V., Kumar, V., Ntwaeaborwa, O., Coetsee, E., Swart, H.: Tunable and white emission from ZnO: $Tb^{3+}$ nanophosphors for solid state lighting applications. Chem. Eng. J. **255**, 541–552 (2014)

Levinson, J., Shepherd, F., Scanlon, P., Westwood, W., Este, G., Rider, M.: Conductivity behavior in polycrystalline semiconductor thin film transistors. J. Appl. Phys. **53**, 1193–1202 (1982)

Li, C., Wang, D., Li, Z., Li, X., Kawaharamura, T., Furuta, M.: Stoichiometry control of ZnO thin film by adjusting working gas ratio during radio frequency magnetron sputtering. J. Mater. **2013**, 1–6 (2013)

Look, D.C., Reynolds, D., Hemsky, J.W., Jones, R., Sizelove, J.: Production and annealing of electron irradiation damage in ZnO. Appl. Phys. Lett. **75**, 811–813 (1999)

Lupan, O., Chow, L., Chai, G., Chernyak, L., Lopatiuk-Tirpak, O., Heinrich, H.: Focused-ion-beam fabrication of ZnO nanorod-based UV photodetector using the in situ lift-out technique. Phys. Stat. Solidi (a) **205**, 2673–2678 (2008a)

Lupan, O., Shishiyanu, S., Chow, L., Shishiyanu, T.: Nanostructured zinc oxide gas sensors by successive ionic layer adsorption and reaction method and rapid photothermal processing. Thin Solid Films **516**, 3338–3345 (2008b)

Lupan, O., Chow, L., Chai, G.: A single ZnO tetrapod-based sensor. Sens. Actuat. B Chem. **141**, 511–517 (2009a)

Lupan, O., Shishiyanu, S., Ursaki, V., Khallaf, H., Chow, L., Shishiyanu, T., Sontea, V., Monaico, E., Railean, S.: Synthesis of nanostructured Al-doped zinc oxide films on Si for solar cells applications. Sol. Energy Mater. Sol. Cells **93**, 1417–1422 (2009b)

Lupan, O., Pauporté, T., Chow, L., Viana, B., Pellé, F., Ono, L., Cuenya, B.R., Heinrich, H.: Effects of annealing on properties of ZnO thin films prepared by electrochemical deposition in chloride medium. Appl. Surf. Sci. **256**, 1895–1907 (2010)

Nagata, T., Ashida, A., Fujimura, N., Ito, T.: The effects of Xe on an rf plasma and growth of ZnO films by rf sputtering. J. Appl. Phys. **95**, 3923–3927 (2004)

Nomura, K., Ohta, H., Ueda, K., Kamiya, T., Hirano, M., Hosono, H.: Thin-film transistor fabricated in single-crystalline transparent oxide semiconductor. Science **300**, 1269–1272 (2003)

Otieno, F., Airo, M., Erasmus, R.M., Billing, D.G., Quandt, A., Wamwangi, D.: Structural and spectroscopic analysis of ex situ annealed RF sputtered aluminium doped zinc oxide thin films. J. Appl. Phys. **122**, 0753031–07530310 (2017)

Özgür, Ü., Alivov, Y.I., Liu, C., Teke, A., Reshchikov, M., Doğan, S., Avrutin, V., Cho, S.-J., Morkoc, H.: A comprehensive review of ZnO materials and devices. J. Appl. Phys. **98**, 041301-1–041301-11 (2005)

Pauporte, T., Rathouský, J.: Electrodeposited mesoporous ZnO thin films as efficient photocatalysts for the degradation of dye pollutants. J. Phys. Chem. C **111**, 7639–7644 (2007)

Pauporté, T., Lincot, D., Viana, B., Pellé, F.: Toward laser emission of epitaxial nanorod arrays of ZnO grown by electrodeposition. Appl. Phys. Lett. **89**, 233112-1–233112-3 (2006)

Reynolds, D., Look, D.C., Jogai, B., Litton, C., Cantwell, G., Harsch, W.: Valence-band ordering in ZnO. Phys. Rev. B **60**, 2340–2344 (1999)

Saravanakumar, K., Gopinathan, C., Mahalakshmi, K., Ganesan, V., Sathe, V., Sanjeeviraja, C.: XPS and Raman studies on (002) oriented nanocrystalline ZnO films showing temperature dependent optical red shift. Adv. Stud. Theor. Phys. **5**, 155–170 (2011)

Spizzirri, P., Fang, J.-H., Rubanov, S., Gauja, E., Prawer, S.: Nano-Raman spectroscopy of silicon surfaces. arXiv preprint http://arxiv.org/abs/1002.2692 (2010)

Sultan, Md, Sultana, N.: Analysis of reflectance and transmittance characteristics of optical thin film for various film materials, thicknesses and substrates. J. Electr. Electron. Syst. **4**, 1–4 (2015)

Szczyrbowski, J., Dietrich, A., Hartig, K.: Bendable silver-based low emissivity coating on glass. Sol. Energy Mater. **19**, 43–53 (1989)

Thanikaikarasan, S., Mahalingam, T., Sundaram, K., Kathalingam, A., Kim, Y.D., Kim, T.: Growth and characterization of electrosynthesized iron selenide thin films. Vacuum **83**, 1066–1072 (2009)

Thomas, D.: The exciton spectrum of zinc oxide. J. Phys. Chem. Solids **15**, 86–96 (1960)

Tominaga, K., Iwamura, S., Fujita, I., Shintani, Y., Tada, O.: Influence of bombardment by energetic atoms on c-axis orientation of ZnO films. Jpn. J. Appl. Phys. **21**, 999–1002 (1982)

Tzolov, M., Tzenov, N., Dimova-Malinovska, D., Kalitzova, M., Pizzuto, C., Vitali, G., Zollo, G., Ivanov, I.: Modification of the structure of ZnO: Al films by control of the plasma parameters. Thin Solid Films **396**, 276–281 (2001)

Valliyil Sasi, V., Iqbal, A., Chaik, K., Iacopi, A., Mohd-Yasin, F.: RF sputtering, post-annealing treatment and characterizations of ZnO (002) thin films on 3C-SiC (111)/Si (111) substrates. Micromachines **8**(148), 2–9 (2017)

Wang, R., Liu, C., Huang, J.-L., Chen, S.-J., Tseng, Y.-K., Kung, S.-C.: ZnO nanopencils: efficient field emitters. Appl. Phys. Lett. **87**, 013110-1–013110-3 (2005)

Willander, M., Nur, O., Zhao, Q., Yang, L., Lorenz, M., Cao, B., Pérez, J.Z., Czekalla, C., Zimmermann, G., Grundmann, M.: Zinc oxide nanorod based photonic devices: recent progress in growth, light emitting diodes and lasers. Nanotechnology **20**, 332001-1–332001-40 (2009)

Yoshida, T., Zhang, J., Komatsu, D., Sawatani, S., Minoura, H., Pauporté, T., Lincot, D., Oekermann, T., Schlettwein, D., Tada, H.: Electrodeposition of inorganic/organic hybrid thin films. Adv. Funct. Mater. **19**, 17–43 (2009)

Youssef, S., Combette, P., Podlecki, J., Asmar, R.A., Foucaran, A.: Structural and optical characterization of ZnO thin films deposited by reactive rf magnetron sputtering. Cryst. Growth Des. **9**, 1088–1094 (2008)

Zhang, J., He, G., Zhu, L., Liu, M., Pan, S., Zhang, L.: Effect of oxygen partial pressure on the structural and optical properties of ZnO film deposited by reactive sputtering. Appl. Surf. Sci. **253**, 9414–9421 (2007)

Springer